AirBender: Adaptive Transportation of Bendable Objects Using Dual UAVs

Jiawei Xu, *Graduate Student Member, IEEE*, Longsen Gao, *Graduate Student Member, IEEE*, Rafael Fierro, *Senior Member, IEEE*, and David Saldaña

***Abstract*—The interaction of robots with bendable objects in midair presents significant challenges in control, often resulting in performance degradation and potential crashes, especially for aerial robots due to their limited actuation capabilities and constant need to remain airborne. This letter presents an adaptive controller that enables two aerial vehicles to collaboratively follow a trajectory while transporting a bendable object without relying on explicit elasticity models. Our method allows on-the-fly adaptation to the object's unknown deformable properties, ensuring stability and performance in trajectory-tracking tasks. We use Lyapunov analysis to demonstrate that our adaptive controller is asymptotically stable. Our method is evaluated through hardware experiments in various scenarios, demonstrating the capabilities of using multirotor aerial vehicles to handle bendable objects.**

***Index Terms*—Aerial systems: Mechanics and control, robust/adaptive control, aerial systems: Applications.**

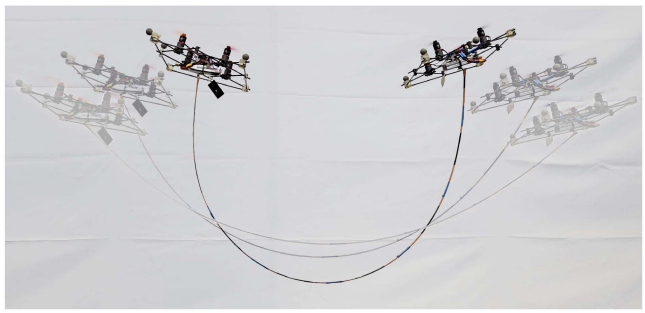

Fig. 1. Two quadrotors actively control the endpoint trajectories of a long carbon-fiber strip using the proposed adaptive controller. **Video:** https://www.youtube.com/watch?v=lhTVIWSjhvQ.

I. Introduction

In RECENT years, multirotor aerial vehicles have rapidly advanced, finding applications in diverse fields such as environmental monitoring, surveillance, package delivery, and search-and-rescue operations. While conventional studies have focused mainly on rigid bodies and point-mass models for multirotor physical interactions [1], [2], real-world scenarios often involve nonrigidity, introducing deformations and elastic properties that significantly influence interaction outcomes [3], [4]. As manipulating bendable objects requires considering deformations and variability in material properties, there are novel potential applications for robots to explore. For example, in agriculture, the deformation of tree branches poses challenges for autonomous cultivation [5]. In autonomous construction, the ability to manipulate bendable materials expands the variety of tasks robots can handle [6], [7]. Our vision is to integrate bendable objects into aerial tasks, enhancing the versatility of aerial vehicles in physical interactions.

Elastic deformation have been studied for almost four centuries [8], and still, they present nontrivial challenges to be incorporated into robotic systems, such as: *i)* Nonlinear deformations are difficult to model and predict [9], [10]; *ii)* real-time sensing and feedback often require accurate detection of the shape and its deformation; *iii)* control algorithms must adapt to the unknown behavior of deformable objects; *iv)* The variability in the physical properties of deformable objects, such as elasticity and stiffness, can change during manipulation. Researchers have made advances to handle these challenges, including the estimation of elastic shapes [11], [12] and the adept manipulation of bendable rods with robotic arms [13]. Model-based analyses often require additional parameters to describe nonrigidity. For example, Kirchhoff and Cosserat deformation models [11] offer generalizability but pose additional analytical challenges compared to the linear elastic rod model [14], [15]. As alternatives, adaptive control [16] and learning [17], [18] make generic assumptions about the characteristics of bendable objects and demonstrate versatility and effectiveness in practical applications.

For transportation purposes, the ability to manipulate nonrigid objects in midair significantly expands the range of objects and applications. However, the natural instability of aerial vehicles requires active stabilization efforts [19]. The presence of external disturbances, such as the elastic force of a bendable rod,

Received 15 September 2024; accepted 13 January 2025. Date of publication 29 January 2025; date of current version 11 February 2025. This article was recommended for publication by Associate Editor C. Gabellieri and Editor G. Loianno upon evaluation of the reviewers' comments. The work of Jiawei Xu and David Saldaña was supported by the NSF under Award 2322840. The work of Longsen Gao and Rafael Fierro was supported by the Air Force Research Laboratory (AFRL) under Grant FA9453-18-2-0022 and Grant FA9550-22-1-0093. *(Corresponding author: Jiawei Xu.)*

Jiawei Xu and David Saldaña are with the Autonomous and Intelligent Robotics Laboratory (AIRLab), Lehigh University, Bethlehem, PA 18015 USA (e-mail: jix519@lehigh.edu; saldana@lehigh.edu).

Longsen Gao and Rafael Fierro are with the Department of Electrical and Computer Engineering, The University of New Mexico, Albuquerque, NM 87131 USA (e-mail: lgao1@unm.edu; rfierro@unm.edu).

This letter has supplementary downloadable material available at https://doi.org/10.1109/LRA.2025.3536276, provided by the authors.

Digital Object Identifier 10.1109/LRA.2025.3536276

IEEE Robotics and Automation Letters (RA-L) paper, presented at ICRA 2026, Vienna, Austria. Cite as RA-L paper.

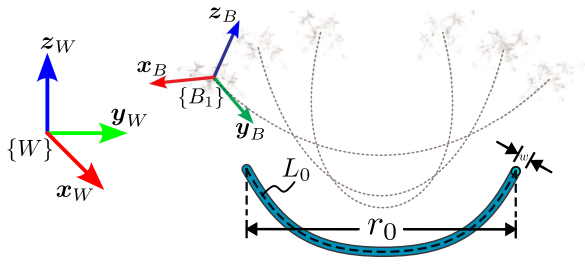

Fig. 2. The vehicles apply forces on two ends of an object, resulting in different bending curves. We consider the world reference frame $\{W\}$ and the body frame of each vehicle, $\{B_1\}$ and $\{B_2\}$.

can lead to manipulation failures or vehicle crashes. Additionally, the computational overhead of intense numerical methods may cause aerial vehicles to destabilize due to the inherent latency sensitivity of their motion control [20]. As a result, few attempts have been made to enable aerial vehicles to manipulate bendable objects in midair, mostly using explicit models of specific elastic objects, both theoretical [21] and practical [22]. We propose an adaptive control approach that allows two aerial vehicles to collaboratively transport a bendable strip in real-time. The object's deformable properties are unknown, and robots are tasked to follow a trajectory while holding the strip from its endpoints.

The main contribution of this letter is the development of a stable trajectory-tracking controller that leverages the recursive least square (RLS) approximation to adapt to an unknown external force from deformation. In comparison to works in multi-robot transportation of rigid payloads [23], [24], [25], [26], our proposed method considers the deformation of the payload and the unknown induced elastic force. Our controller operates without requiring an explicit elasticity model, continuous [27], [28] or discretized [22], [29] and adapts to unknown mass, density, and Young's modulus.

II. Problem Statement

The goal of this work is to transport a bendable object, e.g., a rod, or strip, using two aerial vehicles.

Definition 1 (vehicle): A vehicle is a multirotor with a rigid frame, total weight m, and inertia tensor $\boldsymbol{J}$. Its rotors generate thrust to translate and rotate the vehicle.

The vehicles are located at the ends of the object. We model the connection between each vehicle and the object as a passive spherical joint.

Definition 2 (Bendable object): A bendable object is a long, thin, unstretchable, and incompressible elastic object with a curve length L_0. Its thickness w, mass, m_b, and mass distribution are unknown. The elasticity properties, such as Young's modulus, are also unknown.

Considering the two vehicles connected to the two endpoints of a bendable object, as shown in Fig. 2, we index the two endpoints and the corresponding vehicle with $i = 1, 2$. The body frame $\{B_i\}$ of the vehicle i has its origin fixed at its center of mass (COM). The z-axis of $\{B_i\}$ points in the upward direction of the vehicle, and the x-axis points in the "front" direction of a vehicle. The vehicle generates a force $\boldsymbol{f}_i$ and a torque $\boldsymbol{\tau}_i$.

The position of the i-th vehicle in $\{W\}$ is denoted by $\boldsymbol{p}_i$, and the orientation of $\{B_i\}$ with respect to $\{W\}$ is denoted by the rotation matrix $\boldsymbol{R}_i \in \mathsf{SO}(3)$. We assume that each endpoint is directly fixed in the COM of a vehicle, resulting in the *endpoint displacement vector*, $\boldsymbol{r} = \boldsymbol{p}_2 - \boldsymbol{p}_1$. The magnitude of the endpoint displacement is denoted by $r = \|\boldsymbol{r}\|$, satisfying $0 \leq r \leq L_0$. The vehicles are affected by the object's force $\boldsymbol{f}_i^o$ and torque $\boldsymbol{\tau}_i^o$. Since the object is connected to the COM, the object generates zero torque on the vehicle, i.e., $\boldsymbol{\tau}_i^o = \boldsymbol{0}$.

The object has a natural distance between two endpoints, denoted by r_0, when an external force other than gravity is applied. In this state, $r_0 \leq L_0$ due to the curvature introduced by the bending. When external forces are applied to the endpoints, the object exerts an elastic force as it tends to return to its natural endpoint distance r_0. These characteristics are unknown to the vehicles in our setup, as no explicit elasticity model or knowledge of L_0 or r_0 is assumed.

We describe the vehicle dynamics using Newton-Euler equations,

$$m\ddot{\boldsymbol{p}}_i + mg\boldsymbol{z} = \boldsymbol{f}_i + \boldsymbol{f}_i^o, \tag{1}$$

$$\boldsymbol{J}\dot{\boldsymbol{\omega}}_i + \boldsymbol{\omega}_i \times \boldsymbol{J}\boldsymbol{\omega}_i = \boldsymbol{\tau}_i, \tag{2}$$

where $\dot{\boldsymbol{p}}_i, \ddot{\boldsymbol{p}}_i$ are the linear velocity and acceleration; $\boldsymbol{\omega}_i, \dot{\boldsymbol{\omega}}_i$ are angular velocity and acceleration, respectively. The term g is the gravitational constant.

We assume that the hanging object always lies on a vertical plane $\mathcal{P}$ and does not overlap with itself. The rotational dynamics in (2) is not affected by the object, so an attitude controller that guarantees global stability, such as the geometric controller [30], drives the vehicles to a stable trajectory tracking in the rotational dynamics. However, the unknown object's force $\boldsymbol{f}_i^o$ is not negligible and can lead to instability in the translational dynamics.

Problem (Trajectory tracking for bendable object transportation): Given two vehicles connected to the two endpoints of an unknown bendable object with passive spherical joints, design a control policy, $\boldsymbol{f}_i = \boldsymbol{u}_i$, to track a desired trajectory while adapting to the unknown force of the object, $\boldsymbol{f}_i^o$.

There are three major challenges in addressing the Problem. First, the object's response to a vehicle's force is unknown and can cause instability. Second, the lack of direct sensor measurements of the bendable force requires a force observer, of which the noise may harm the trajectory tracking performance. Third, the low-latency requirement from the vehicles advocates a real-time method that is computationally light.

The force compensation for bending the object is critical to trajectory tracking quality since the object force $\boldsymbol{f}_i^o$ directly influences the translational dynamics, as shown in (1). Thus, the primary objective is to design a control policy $\boldsymbol{u}_i$ such that it adapts to the unknown bending force while tracking a trajectory. A key intuition about bendable objects is that a greater deformation requires a larger bending force, linking the force to the vehicles' states. Therefore, without an explicit model of the bendable object, the aerial vehicles can adapt by estimating the unknown force using their states, and use an acceleration observer to continuously update the estimation, and further refine the adaptation.

IEEE Robotics and Automation Letters (RA-L) paper, presented at ICRA 2026, Vienna, Austria. Cite as RA-L paper.

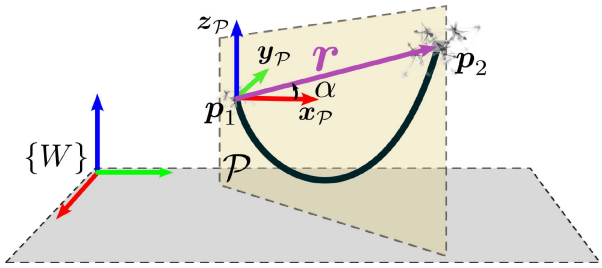

Fig. 3. The strip lies in a vertical plane $\mathcal{P}$, the displacement of its two endpoints being $\boldsymbol{r}$.

III. Adaptive Controller

We approach the Problem using adaptive control [16] and model the object's force, $\boldsymbol{f}_i^o$, as a function of the vehicle states.

A. Trajectory-Tracking Control Via Force Adaptation

We estimate the force $\boldsymbol{f}_i^o$ using recursive least-square approximation [31]. Since the bendable object force depends on its endpoint displacement $\boldsymbol{r}$, and the positional constraints ensure that the object curve remains in the same plane, we model an approximation function that maps the displacement to the required force.

We assume that the object's plane, $\mathcal{P}$, is vertical, i.e., $\boldsymbol{z}_\mathcal{P} = \boldsymbol{z} \in \mathcal{P}$, as illustrated in Fig. 3. This assumption allows us to approximate the orientation of $\mathcal{P}$ with only the knowledge of the endpoint positions of the rod, which is suitable for the scenario where the "swinging" behavior caused by the vehicle motion is neglectable. The displacement vector $\boldsymbol{r}$ determines the unit normal vector of $\mathcal{P}$, $\boldsymbol{y}_\mathcal{P} = \frac{\boldsymbol{r}\times\boldsymbol{z}_\mathcal{P}}{\|\boldsymbol{r}\times\boldsymbol{z}_\mathcal{P}\|}$. The horizontal unit basis vector of $\mathcal{P}$ is $\boldsymbol{x}_\mathcal{P} = \boldsymbol{y}_\mathcal{P} \times \boldsymbol{z}_\mathcal{P}$. Therefore, the orientation of $\mathcal{P}$ with respect to the world frame is $\boldsymbol{R}_\mathcal{P} = \begin{bmatrix}\boldsymbol{x}_\mathcal{P} & \boldsymbol{y}_\mathcal{P} & \boldsymbol{z}_\mathcal{P}\end{bmatrix}$. The displacement vector on $\mathcal{P}$ is then $\boldsymbol{r}_\mathcal{P} = \boldsymbol{R}_\mathcal{P}^\top \boldsymbol{r}$. The object's force projected on the plane $\mathcal{P}$ is denoted by $\boldsymbol{f}_{i,\mathcal{P}}^o$. Then, we denote the estimator of $\boldsymbol{f}_{i,\mathcal{P}}^o$ by $\hat{\boldsymbol{f}}_{i,\mathcal{P}}^o$, of which the projection in the world frame is $\hat{\boldsymbol{f}}_i^o = \boldsymbol{R}_\mathcal{P}\hat{\boldsymbol{f}}_{i,\mathcal{P}}^o$. We model the force $\boldsymbol{f}_{i,\mathcal{P}}^o$ as a mapping of a nonlinear feature vector $\boldsymbol{\phi}$ that depends on the vehicles' state,

$$\boldsymbol{f}_{i,\mathcal{P}}^o = \boldsymbol{W}_i^\top \boldsymbol{\phi}, \tag{3}$$

where $\boldsymbol{W}_i \in \mathbb{R}^{(4n+1)\times 3}$ is the weight matrix. Since the deformation and the bending force, is smooth and continuous on a closed interval, a polynomial of the endpoint displacement $\boldsymbol{r}_\mathcal{P}$ uniformly approximates the function as accurately as desired, based on the Stone-Weierstrass Theorem [32]. We use an n-th order polynomial feature of nonzero elements in $\boldsymbol{r}_\mathcal{P}$ and $\dot{\boldsymbol{r}}_\mathcal{P}$,

$$\boldsymbol{\phi} = \left[r_x^n, r_x^{n-1}, \ldots, r_x, r_z^n, \ldots, r_z, \dot{r}_x^n, \ldots, \dot{r}_x, \dot{r}_z^n, \ldots, \dot{r}_z, 1\right]^\top, \tag{4}$$

where r_x, r_z are the first and third element of $\boldsymbol{r}_\mathcal{P}$. $\dot{r}_x$, $\dot{r}_z$ are the first and third element of $\dot{\boldsymbol{r}}_\mathcal{P}$, respectively. We highlight that the use of polynomials requires fewer terms than other approximation functions such as neural networks. We use continuous Recursive Least-Square algorithm [33], [34] to update the approximation, $\hat{\boldsymbol{W}}_i$, of the unknown weight matrix $\boldsymbol{W}_i$, so that the estimator

$$\hat{\boldsymbol{f}}_{i,\mathcal{P}}^o = \hat{\boldsymbol{W}}_i^\top \boldsymbol{\phi} \tag{5}$$

converges to $\boldsymbol{f}_{i,\mathcal{P}}^o$ as the sample size becomes infinite. Since the object's force cannot be easily measured directly, we use an acceleration-based force observer to obtain it based on the vehicle dynamics in (1),

$$\boldsymbol{f}_i^o = m\ddot{\boldsymbol{p}}_i + mg\boldsymbol{z} - \boldsymbol{u}_i, \tag{6}$$

where the vehicle's force $\boldsymbol{u}_i$ can be computed based on the actuator inputs, and the vector $\ddot{\boldsymbol{p}}_i$ can be measured. In practice, the measurement is noisy due to the nature of taking double derivatives on the measured position and noisy measurements from the inertial sensor. In addition, the measurement is only available after motor actuation and the states are observed. To ensure the trajectory tracking controller addresses the bendable force while taking action, we estimate the force based on the expected states before measurement, and update the estimation based on the measurement.

We initialize the weight matrix as a zero matrix, $\hat{\boldsymbol{W}}_i(0) = \boldsymbol{0}$, and the covariance as the identity matrix, $\boldsymbol{P}_i(0) = \boldsymbol{I}$. The update rule given by the continuous-time recursive least-square algorithm with a forgetting factor [31] is,

$$\dot{\hat{\boldsymbol{W}}}_i = \boldsymbol{P}_i\boldsymbol{\phi}\,\boldsymbol{\epsilon}_i^\top \tag{7}$$

$$\dot{\boldsymbol{P}}_i = \lambda\boldsymbol{P}_i - \boldsymbol{P}_i\boldsymbol{\phi}_i\boldsymbol{\phi}_i^\top\boldsymbol{P}_i \tag{8}$$

where the force estimation error in $\mathcal{P}$ is

$$\boldsymbol{\epsilon}_i = \boldsymbol{R}_\mathcal{P}^\top\boldsymbol{f}_i^o - \hat{\boldsymbol{f}}_{i,\mathcal{P}}^o. \tag{9}$$

Using the updated weight matrix, the vehicles track the desired trajectories while adapting to the elastic force simultaneously.

The objective of our control policy is to track each endpoint of the object to a desired trajectory $\boldsymbol{p}_i^d$ by driving the position error, $\boldsymbol{e}_i = \boldsymbol{p}_i^d - \boldsymbol{p}_i$, and velocity error, $\dot{\boldsymbol{e}}_i = \dot{\boldsymbol{p}}_i^d - \dot{\boldsymbol{p}}_i$, to zero, while adapting to the object's unknown force. Our proposed control policy combines the proportional-derivative trajectory tracking controller and the force adaptation,

$$\boldsymbol{u}_i = k_p\boldsymbol{e}_i + k_d\dot{\boldsymbol{e}}_i + mg\boldsymbol{z} + m\ddot{\boldsymbol{p}}^d - \hat{\boldsymbol{f}}_i^o, \tag{10}$$

where $k_p, k_d > 0$ are scalar proportional and derivative gains for the errors. The trajectory desired acceleration $\ddot{\boldsymbol{p}}^d$ is the feedforward term. We estimate the object's force $\hat{\boldsymbol{f}}_{i,\mathcal{P}}^o$ on the $\mathcal{P}$ plane using the least-square approximation and project it back to the world frame to obtain $\hat{\boldsymbol{f}}_i^o$. Although a PID controller can use the accumulated error to compensate for the bending force, it would work when the bending force is constant, otherwise, the changes in the bending force can lead to oscillations, delays, and instability.

For the approximated weight matrix $\hat{\boldsymbol{W}}_i$ to converge to the actual matrix $\boldsymbol{W}_i$, the input $\sum_{q=t}^{t+N-1}\boldsymbol{\phi}(q)\boldsymbol{\phi}(q)^\top$ must be persistently excited (PE) [31]. To satisfy PE, we can design trajectories with diverse motion, typically by using periodic or aperiodic signals that span a broad frequency range. Alternatively, we can superimpose oscillatory components at varying frequencies onto the original trajectories. Consequently, the collected data

IEEE Robotics and Automation Letters (RA-L) paper, presented at ICRA 2026, Vienna, Austria. Cite as RA-L paper.

becomes informative enough to maintain a full-rank sum of outer products, guaranteeing the controller's convergence and stability.

B. Stability

Based on the assumption that our force estimation model in (3) is sufficiently accurate to an arbitrary precision of choice according to Stone-Weierstrass Theorem, we study the stability of the system described in (1) using our control input in (10) in the task of trajectory tracking,

$$m\ddot{\boldsymbol{p}}_i = k_p \boldsymbol{e}_i + k_d \dot{\boldsymbol{e}}_i + m\ddot{\boldsymbol{p}}^d + \boldsymbol{f}_i^o - \hat{\boldsymbol{f}}_i^o, \tag{11}$$

where $\boldsymbol{f}_i^o = \boldsymbol{R}_{\mathcal{P}} \boldsymbol{W}_i^\top \boldsymbol{\phi}$. We rearrange the terms and include the force estimation in $\mathcal{P}$ with (3) and (5) to obtain

$$m\ddot{\boldsymbol{e}}_i = -k_d \dot{\boldsymbol{e}}_i - k_p \boldsymbol{e}_i + \boldsymbol{R}_{\mathcal{P}} \tilde{\boldsymbol{W}}_i^\top \boldsymbol{\phi}, \tag{12}$$

where $\tilde{\boldsymbol{W}}_i = \boldsymbol{W}_i - \hat{\boldsymbol{W}}_i$ is the weight matrix error, which we can use to rewrite the force estimation error as

$$\boldsymbol{\epsilon}_i = \tilde{\boldsymbol{W}}_i^\top \boldsymbol{\phi}. \tag{13}$$

We define a candidate Lyapunov function considering the error dynamics and the estimation error,

$$V_i = V_i^p + V_i^W, \quad \text{where} \tag{14}$$

$$V_i^p = \frac{1}{2} m \dot{\boldsymbol{e}}_i^\top \dot{\boldsymbol{e}}_i + \frac{1}{2} \boldsymbol{e}_i^\top k_p \boldsymbol{e}_i, \tag{15}$$

$$V_i^W = \mathrm{tr}(\tilde{\boldsymbol{W}}_i^\top \boldsymbol{P}_i^{-1} \tilde{\boldsymbol{W}}_i). \tag{16}$$

The operator $\mathrm{tr}(\cdot)$ denotes the trace of a matrix. Note that V_i^p is associated with the tracking error and V_i^W is with the estimation error. Since the proportional gain k_p and the inverse covariance matrix $\boldsymbol{P}$ are both positive definite, the Lyapunov candidate is positive definite. If and only if the position error $\boldsymbol{e}_i = \boldsymbol{0}$, the position error derivative $\dot{\boldsymbol{e}}_i = \boldsymbol{0}$, and the weight matrix error $\tilde{\boldsymbol{W}}_i = \boldsymbol{0}$ are zero, the candidate $V_i = 0$ is zero.

The derivative of the Lyapunov candidate, $\dot{V}_i = \dot{V}_i^p + \dot{V}_i^W$ contains two major components. First, we simplify the derivative of the estimation component,

$$\dot{V}_i^W = 2\mathrm{tr}(\tilde{\boldsymbol{W}}_i^\top \boldsymbol{P}_i^{-1} \dot{\tilde{\boldsymbol{W}}}_i) + \mathrm{tr}\left(\tilde{\boldsymbol{W}}_i^\top \frac{d}{dt}(\boldsymbol{P}_i^{-1}) \tilde{\boldsymbol{W}}_i \right). \tag{17}$$

The weight matrix update rule in (7) induces $\dot{\tilde{\boldsymbol{W}}}_i = -\dot{\hat{\boldsymbol{W}}}_i = -\boldsymbol{P}_i \boldsymbol{\phi} \boldsymbol{\epsilon}_i^\top$. Assuming $\lambda = 0$ for the recursive least-squares without forgetting factor, the covariance matrix update rule in (8) gives $\dot{\boldsymbol{P}}_i = -\boldsymbol{P}_i \boldsymbol{\phi}_i \boldsymbol{\phi}_i^\top \boldsymbol{P}_i$. Combined with the identity $\frac{d}{dt}(\boldsymbol{P}_i^{-1} \boldsymbol{P}_i) \equiv \boldsymbol{0}$, which gives $\frac{d}{dt}(\boldsymbol{P}_i^{-1}) = -\boldsymbol{P}_i^{-1} \dot{\boldsymbol{P}}_i \boldsymbol{P}_i^{-1}$, we simplify (17) into

$$\begin{aligned}
\dot{V}_i^W &= -2\mathrm{tr}(\tilde{\boldsymbol{W}}_i^\top \boldsymbol{\phi} \boldsymbol{\epsilon}_i^\top) - \mathrm{tr}(\tilde{\boldsymbol{W}}_i^\top \boldsymbol{P}_i^{-1} \dot{\boldsymbol{P}}_i \boldsymbol{P}_i^{-1} \tilde{\boldsymbol{W}}_i) \\
&= -2\mathrm{tr}(\tilde{\boldsymbol{W}}_i^\top \boldsymbol{\phi} \boldsymbol{\epsilon}_i^\top) \\
&\quad - \mathrm{tr}(\tilde{\boldsymbol{W}}_i^\top \boldsymbol{P}_i^{-1} (-\boldsymbol{P}_i \boldsymbol{\phi}_i \boldsymbol{\phi}_i^\top \boldsymbol{P}_i) \boldsymbol{P}_i^{-1} \tilde{\boldsymbol{W}}_i) \\
&= -2\mathrm{tr}(\boldsymbol{\epsilon}_i \boldsymbol{\epsilon}_i^\top) + \mathrm{tr}(\boldsymbol{\epsilon}_i \boldsymbol{\epsilon}_i^\top) \\
&= -\boldsymbol{\epsilon}_i^\top \boldsymbol{\epsilon}_i < 0,
\end{aligned} \tag{18}$$

which is negative definite. If and only if the force estimation error $\|\boldsymbol{\epsilon}_i\| = 0$ is zero, this derivative component of the Lyapunov function is zero. Combined with the positive definiteness of V_i^W from (16), it shows the global asymptotic attraction of the estimation error to zero. The second component is the derivative related to tracking errors,

$$\dot{V}_i^p = m \dot{\boldsymbol{e}}_i^\top \ddot{\boldsymbol{e}}_i + \boldsymbol{e}_i^\top \, k_p \dot{\boldsymbol{e}}_i. \tag{19}$$

Substituting $\ddot{\boldsymbol{e}}$ with the error dynamics in (12), we obtain

$$\begin{aligned}
\dot{V}_i^p &= \dot{\boldsymbol{e}}_i^\top \left(\boldsymbol{R}_{\mathcal{P}} \tilde{\boldsymbol{W}}_i^\top \boldsymbol{\phi} - k_p \boldsymbol{e}_i - k_d \dot{\boldsymbol{e}}_i \right) + \boldsymbol{e}_i^\top k_p \dot{\boldsymbol{e}}_i \\
&= \dot{\boldsymbol{e}}_i^\top \boldsymbol{R}_{\mathcal{P}} \tilde{\boldsymbol{W}}_i^\top \boldsymbol{\phi} - \dot{\boldsymbol{e}}_i^\top k_d \dot{\boldsymbol{e}}_i \\
&= \dot{\boldsymbol{e}}_i^\top \boldsymbol{R}_{\mathcal{P}} \boldsymbol{\epsilon}_i - \dot{\boldsymbol{e}}_i^\top k_d \dot{\boldsymbol{e}}_i.
\end{aligned} \tag{20}$$

The Lyapunov function as a result of the derivation of its two components in (18) and (20) is,

$$\begin{aligned}
\dot{V}_i &= \dot{V}_i^W + \dot{V}_i^p \\
&= -\boldsymbol{\epsilon}_i^\top \boldsymbol{\epsilon}_i + \dot{\boldsymbol{e}}_i^\top \boldsymbol{R}_{\mathcal{P}} \boldsymbol{\epsilon}_i - \dot{\boldsymbol{e}}_i^\top k_d \dot{\boldsymbol{e}}_i.
\end{aligned} \tag{21}$$

The right-hand side of (21) is composed of two negative squares and $\dot{\boldsymbol{e}}_i^\top \boldsymbol{R}_{\mathcal{P}} \boldsymbol{\epsilon}_i$. Since the rotation matrix $\boldsymbol{R}_{\mathcal{P}}$ changes only the direction of the vector $\boldsymbol{\epsilon}_i$, the maximum value of $\dot{\boldsymbol{e}}_i^\top \boldsymbol{R}_{\mathcal{P}} \boldsymbol{\epsilon}_i$ is bounded by $\|\dot{\boldsymbol{e}}_i\| \|\boldsymbol{\epsilon}_i\|$ when $\dot{\boldsymbol{e}}_i$ is co-linear with $\boldsymbol{R}_{\mathcal{P}} \boldsymbol{\epsilon}_i$, i.e.,

$$\dot{V}_i \leq -\|\boldsymbol{\epsilon}_i\|^2 + \|\dot{\boldsymbol{e}}_i\| \|\boldsymbol{\epsilon}_i\| - k_d \|\dot{\boldsymbol{e}}_i\|^2 \tag{22}$$

We can reorganize the right-hand side of (22) into the summation of two negative square terms,

$$\dot{V}_i \leq -\left(\|\boldsymbol{\epsilon}_i\| - \frac{1}{2} \|\dot{\boldsymbol{e}}_i\| \right)^2 - \left(k_d - \frac{1}{4} \right) \|\dot{\boldsymbol{e}}_i\|^2 < 0, \tag{23}$$

which is negative definite for $k_d > \frac{1}{4}$. If and only if both the velocity tracking error $\dot{\boldsymbol{e}}_i = \boldsymbol{0}$ and the force estimation error $\boldsymbol{\epsilon}_i = \boldsymbol{0}$ are zero, the Lyapunov derivative is zero. As a result, we have the Lyapunov function V_i positive definite, and its derivative $\dot{V}_i$ negative definite for $k_d > \frac{1}{4}$. When the tracking errors and the force estimation error are both zero, $V_i = 0$. Since the feature vector $\boldsymbol{\phi}$ is a polynomial of the bounded endpoint displacement, the magnitude of the weight matrix error is bounded. Likewise, the magnitude of the position and velocity errors for the task of trajectory-tracking is bounded. Thus, the system of aerial vehicles and the bendable object is *asymptotically stable* in tracking the endpoint trajectories while compensating for the object's force. It is noted that depending on the order of polynomial and the model mismatch unaccounted for such as the misalignment from the vehicle CoM and the connection point to the bendable object, the force estimation model is not accurate in practice. Consequently, the force estimation error $\boldsymbol{\epsilon_i}^\top \boldsymbol{\epsilon_i}$ in $\mathcal{P}$ will stabilize around 0, resulting in a residual trajectory tracking error. Though a feature vector of higher polynomial order offers lower estimation errors, it also increases the computation overhead as the size of $\hat{\boldsymbol{W}}_i$ increases. An alternative to lower the estimation error is to adopt a different feature vector which incorporates the physical insights of a bendable objects.

IEEE Robotics and Automation Letters (RA-L) paper, presented at ICRA 2026, Vienna, Austria. Cite as RA-L paper.

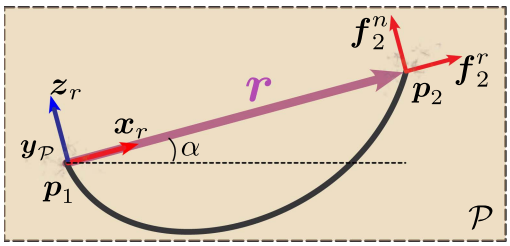

Fig. 4. The object force in parallel and perpendicular to displacement vector in the plane $\mathcal{P}$. The force vectors on vehicle 1 omitted for illustration clarity.

C. Physical Insights of a Bendable Object

The most fundamental physical characteristic of a bendable object is its tendency to recover its endpoint displacement r to the natural value r_0. When the object is bent, $r \neq r_0$ leads the object to resist bending, resulting in the elastic force received by the vehicles. During transportation, the vehicles also need to take into account the force due to gravity, which is nontrivial because of its unknown mass distribution. The gravity compensation of each vehicle depends on the leaning of the object, α, which is the angle between $\boldsymbol{r}$ and the horizontal plane,

$$\alpha = \arctan\left(\frac{\boldsymbol{r}\cdot\boldsymbol{z}_\mathcal{P}}{\boldsymbol{r}\cdot\boldsymbol{x}_\mathcal{P}}\right). \tag{24}$$

These insights motivate us to construct a new feature vector for improved force estimation. We first decompose the total force received by the vehicles from the object in parallel and perpendicular to the displacement vector $\boldsymbol{r}$, that is, $\boldsymbol{f}_i^r$ and $\boldsymbol{f}_i^n$ at endpoint i, as shown in Fig. 4. As such, the external force applied by the object is $\boldsymbol{f}_i^o = \boldsymbol{f}_i^r + \boldsymbol{f}_i^n$. To ensure that this modification is consistent with the methods introduced in Section III-A, we find the unit vector of the displacement $\boldsymbol{x}_r = \frac{\boldsymbol{r}}{\|\boldsymbol{r}\|}$, and the normal vector of $\boldsymbol{x}_r$ in $\mathcal{P}$, $\boldsymbol{z}_r = \mathrm{Rot}(\boldsymbol{y}_\mathcal{P}, -\frac{\pi}{2})\boldsymbol{x}_r$ by applying Rodrigues' rotation formula. Thus, we obtain the rotation matrix $\boldsymbol{R}_o \triangleq \begin{bmatrix}\boldsymbol{x}_r & \boldsymbol{y}_\mathcal{P} & \boldsymbol{z}_r\end{bmatrix}$ using the three orthogonal unit vectors. This rotation matrix, combined with a selected origin at $\boldsymbol{p}_1$, defines a new frame $\{O\}$, of which the xz-plane is identical to $\mathcal{P}$ with a different set of basis vectors. By projecting $\boldsymbol{f}_i^o$ into $\{O\}$, we obtain $\boldsymbol{f}_{i,o}^o = \boldsymbol{R}_o^\top \boldsymbol{f}_i^o$, of which the first and third elements are the magnitudes of $\boldsymbol{f}_i^r$ and $\boldsymbol{f}_i^n$. We define the feature vector

$$\boldsymbol{\phi}^b = \big[r^n, r^{n-1}, \ldots, r, \dot{r}^n, \ldots, \dot{r}, \cos n\alpha, \ldots, \cos\alpha, \sin n\alpha, \ldots, \sin\alpha, 1\big]^\top. \tag{25}$$

We model the object force in $\{O\}$ as a linear function of the new feature vector $\boldsymbol{\phi}^b$, i.e., $\boldsymbol{f}_{i,o}^o = \boldsymbol{W}_i^b \boldsymbol{\phi}^b$. The estimator of $\boldsymbol{f}_{i,o}^o$ is denoted by $\hat{\boldsymbol{f}}_{i,o}^o = \hat{\boldsymbol{W}}_i^b \boldsymbol{\phi}^b$ and $\hat{\boldsymbol{W}}_i^b \in \mathbb{R}^{(4n+1)\times 3}$ is the associated estimation weight matrix. While the update rules remain the same as in (7), (8), the estimation error is

$$\boldsymbol{\epsilon}_i^b = \boldsymbol{R}_o^\top \boldsymbol{f}_i^o - \hat{\boldsymbol{f}}_{i,o}^o. \tag{26}$$

This new feature vector takes into consideration the physical characteristics of a bendable object without explicit knowledge of the model, thus generalizes over different bendable objects. The stability proof follows the same procedure as in Section III-B by replacing $\boldsymbol{R}_\mathcal{P}$ with $\boldsymbol{R}_o$. The performance of both feature vectors is evaluated in the next section.

IV. Experiments

We connect a quadrotor to each endpoint of a thin and long carbon-fiber strip and use the two quadrotors to drive the bendable object's endpoints to follow a desired trajectory to validate our methods. A snapshot of the experiments is shown in Fig. 1. We measure the performance in terms of position tracking errors and compare the performance of our adaptive control to that of the standard PID control. We evaluate the methods using three different trajectories. For simplicity, we refer to the system of the two quadrotors and the bendable strip as "the system" in this section.

We use the quadrotor modules from the H-ModQuad project [35] as the aerial vehicle. Each module weighs 135 g and has a payload capacity of over 100 g. A ground station calculates and sends the trajectory waypoints to the quadrotors using the Crazyswarm [36] framework at 100 Hz. The ground station executes the RLS calculation and sends the compensation force for bending to the quadrotors consistently throughout an experiment. The strip for the experiments is constructed as a composite of multiple carbon fiber strips of different weights, thicknesses, base shapes, and lengths to achieve asymmetry and nonhomogeneity.[1]

A. Trajectory-Tracking Evaluation

In the first experiment, we command the system to translate in x-direction at a constant speed while maintaining height and the $\mathcal{P}$ plane orientation, The endpoint distance of the strip varies sinusoidally, and the desired height of both endpoints oscillates at different frequencies with a magnitude of 0.05 m. The strip has a curve length of $L_0 = 1.2$ m and a natural endpoint displacement $r_0 = 1.05$ m. During transportation, we command the quadrotors to oscillate the endpoint displacement between 0.8 m and 0.4 m. This trajectory evaluates the strength and convergence speed of the force compensation methods during strip bending. Using our adaptive controller, the system can quickly and consistently reduce tracking errors that are significantly smaller than the PID baseline. We run the trajectory 10 times with each method for 40 seconds each time. For adaptive controllers, we continue to update the RLS matrices, i.e., $\boldsymbol{W}_i$ and $\boldsymbol{P}_i$, across the trials. The mean and standard deviation (STD) of the average tracking errors of the two endpoints over time are shown in Fig. 5. The mean and STD of the average tracking errors of the two endpoints over the 10 trials are shown in Fig. 6.

We highlight three observations. First, while the PID baseline consistently achieves a mean error around 0.13 m with an STD of 0.03 m, our adaptive controllers with both feature vectors achieve a lower mean error less than 0.1 m with an STD of 0.04 m during the first trial, and eventually achieve a *significantly* lower mean error less than 0.05 m with an STD of 0.02 m. Second, since the PID controller compensates for the

[1]The complete set of video and data recordings is available at https://tinyurl.com/bendables.

IEEE Robotics and Automation Letters (RA-L) paper, presented at ICRA 2026, Vienna, Austria. Cite as RA-L paper.

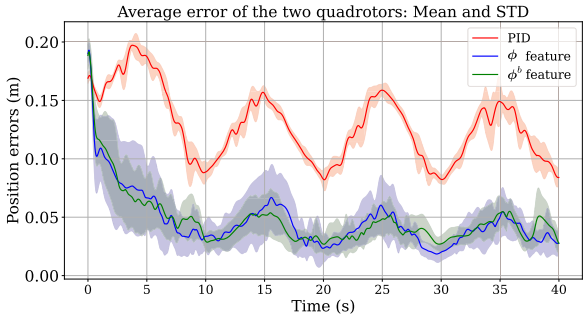

Fig. 5. The mean and standard deviation of the average endpoint position errors v.s. time for tracking a varying endpoint distance.

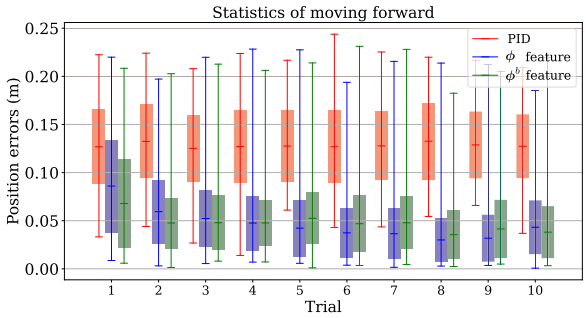

Fig. 6. The mean and standard deviation of the average endpoint position errors v.s. trial for tracking a varying endpoint distance.

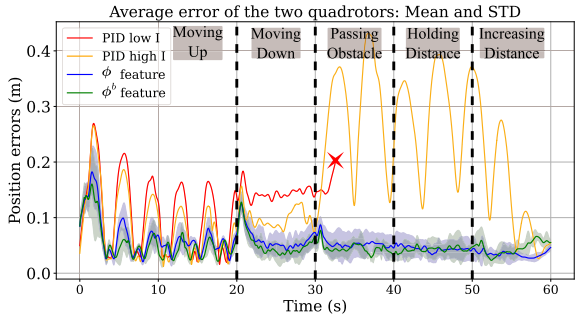

Fig. 7. The mean and STD of the average endpoint position errors v.s. time for climbing up and passing one obstacle. The red cross marks where the PID controller with a low integral term fails to drive the strip through the obstacle.

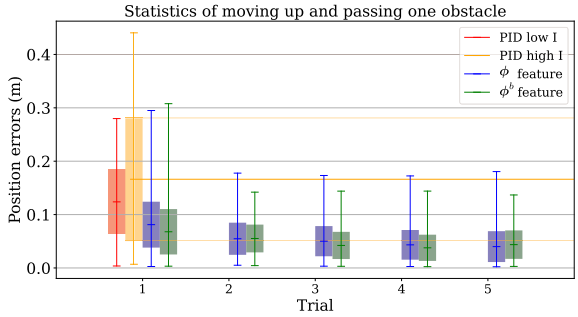

Fig. 8. The mean and standard deviation of the average endpoint position errors v.s. trial for climbing up and passing one obstacle.

bendable force by accumulating the integral term, it does not comprehend the characteristics of the bendable strip, resulting in a high deviation in error. In contrast, our controller learns the bendable force by updating the weight matrices, thus achieving a lower deviation. Third, the ϕ^b feature vector provides a deeper understanding of the bendable characteristics, which leads to faster convergence and lower errors compared to using the ϕ feature vector. In addition, we assume that a quadrotor connects to the object's endpoint at its CoM, and thus the bendable object applies zero torque on the quadrotors. However, in practice, slight deviations in the connection point from the quadrotor CoM create unexpected torques. These torques amplify errors both in force compensation magnitude and direction in the PID baseline, which results in higher tracking errors as bending the object more requires higher force.

B. Simple Task: Passing Through a Window

In the second experiment, we design a trajectory to move forward-up, and then pass through a square window. It is composed of five parts. First, the system translates in x-direction at a constant speed, moves up, and maintains the $\mathcal{P}$ -plane orientation at the same time until the system reaches a height of 1.8 m. The upward movement is combined with a varying endpoint distance between 0.6 m and 1.1 m sinusoidally, and both endpoints change their relative heights to the system height sinusoidally at different frequencies with a magnitude of 0.05 m. Second, the system maintains the endpoint displacement distance at 0.6 m and moves down in the z-direction while maintaining the $\mathcal{P}$ orientation and the x -axis speed until the height reaches 0.7 m. Third, the two quadrotors maintain the endpoint displacement while moving forward to pass through the square obstacle. Fourth, after going through the obstacle, the system stays static for 10s. Lastly, the system increases the displacement distance to the same value during takeoff, then lands, finishing the task.

The results in terms of position errors are shown in Figs. 7 and 8. We run the PID baselines only once since their performance does not improve with repetitions. The PID baseline with the default low integral term for unconstrained quadrotors fails to pass through the obstacle as error integration does not generate enough force to bend the strip timely, marked by a red cross in Fig. 7. PID with twice as high of the default integral term succeeds in passing the obstacle but struggles to damp the position error when the quadrotors are commanded to stay static while bending the strip. The adaptive controllers with both feature vectors complete the task and maintain the average position error below 0.05 m after 3 trials, with an STD less than 0.03 m. The task lasts 60 s, which is 20 s longer than Exp. IV-A. The longer runtime allows the adaptive controllers to converge further to a lower error within the first trial. Similar observation as in Section IV-A holds that using ϕ^b feature vector fosters a faster convergence than using ϕ.

C. Complex Task: Traversing Two Perpendicular Windows

In the third experiment, both quadrotors first follow an obstacle-free trajectory for 60 seconds to maintain persistence of excitation. The trajectory varies the endpoint displacement

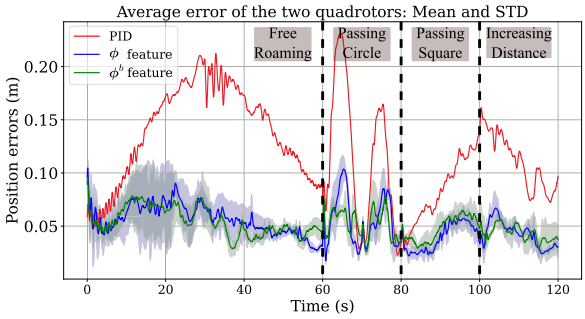

Fig. 9. The mean and standard deviation of the average endpoint position errors v.s. time for passing two obstacles.

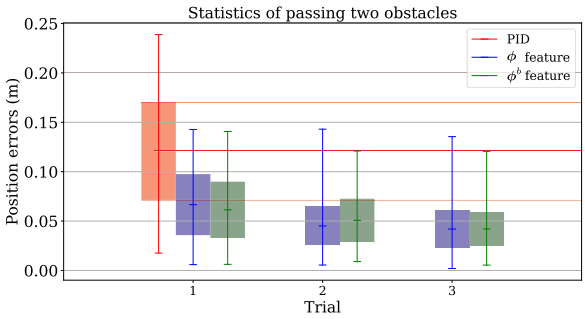

Fig. 10. The mean and standard deviation of the average endpoint position errors v.s. trial for passing two obstacles.

between 0.4 m and 1.0 m with a sinusoidal function, changes the heights of both endpoints at different frequencies with a magnitude of 0.1 m, completes a full 2π revolution of $\mathcal{P}$, and makes the oscillatory translation of both endpoints in x- and y -axes with a magnitude of 4.0m and 0.2m, respectively. In the second 60-second period, the two quadrotors transport the bendable strip to pass through a circular window while bending it with a fixed $\mathcal{P}$ orientation, then pass through a second square window with a varying $\mathcal{P}$ orientation. Then, the quadrotors recover the endpoint displacement to the take-off value before landing. This 120-second experiment emulates real-world scenarios where two quadrotors transport a bendable object through a cluttered environment while constantly bending it to avoid collisions.

The results of three trials using the adaptive controllers and the baseline PID controller are shown in Figs. 9 and 10. Overall, our adaptive controllers with both feature vectors converge to a mean error half that achieved by the PID controller in the first trial and continue to achieve significantly lower errors than the PID controller in the follow-up experiments. The results demonstrate the effectiveness of our adaptive controller in realistic settings. Since the integral term only compensates for accumulated error in the world frame, it does not account for the changing orientation of the displacement vector presented in this experiment. Consequently, our adaptive controller achieves significantly higher performance facing varying force directions in the world frame than the PID baseline.

V. Conclusion

In this letter, we presented the problem of using aerial vehicles to transport a bendable object. Due to the limited actuation capabilities of aerial vehicles and their need to maintain airborne stability, the unknown elastic forces resulting from bending the object might lead to crashes if not properly addressed. We modeled the unknown force as a parametric function of the bendable object's endpoint displacement and proposed an adaptive controller based on recursive least squares to estimate the force. By integrating the force adaptation into the trajectory tracking controller, we derived a novel controller that allows aerial vehicles to transport the bendable object while adapting to the elastic forces in real time. Through Lyapunov analysis, we proved the stability of the trajectory tracking and the convergence of parameter approximation for force adaptation. We demonstrated the effectiveness of our methods with real quadrotors and carbon-fiber strips in extensive experiments featuring different trajectories. In all tests, our adaptive controller significantly outperformed the PID controller, achieving smaller errors. In future work, we aim to extend this method to account for different object shapes, numbers of robots, and high-speed maneuvers.

Acknowledgment

Any opinions findings, and conclusions or recommendations expressed in this material are those of the authors and do not necessarily reflect the views of the United States Air Force.

References

[1] M. Fumagalli et al., "Developing an aerial manipulator prototype: Physical interaction with the environment," *IEEE Robot. Automat. Mag.*, vol. 21, no. 3, pp. 41–50, Sep. 2014.
[2] M. Ryll et al., "6D physical interaction with a fully actuated aerial robot," in *Proc. 2017 IEEE Int. Conf. Robot. Automat.*, 2017, pp. 5190–5195.
[3] V. E. Arriola-Rios, P. Guler, F. Ficuciello, D. Kragic, B. Siciliano, and J. L. Wyatt, "Modeling of deformable objects for robotic manipulation: A tutorial and review," *Front. Robot. AI*, vol. 7, 2020, Art. no. 82.
[4] H. Yin, A. Varava, and D. Kragic, "Modeling, learning, perception, and control methods for deformable object manipulation," *Sci. Robot.*, vol. 6, no. 54, 2021, Art. no. eabd8803.
[5] J. Jacob, T. Bandyopadhyay, J. Williams, P. Borges, and F. Ramos, "Learning to simulate tree-branch dynamics for manipulation," *IEEE Robot. Automat. Lett.*, vol. 9, no. 2, pp. 1748–1755, Feb. 2024.
[6] P. Radoglou-Grammatikis, P. Sarigiannidis, T. Lagkas, and I. Moscholios, "A compilation of UAV applications for precision agriculture," *Comput. Netw.*, vol. 172, 2020, Art. no. 107148.
[7] J. Cortsen, J. A. Jørgensen, D. Sølvason, and H. G. Petersen, "Simulating robot handling of large scale deformable objects: Manufacturing of unique concrete reinforcement structures," in *Proc. 2012 IEEE Int. Conf. Robot. Automat.*, 2012, pp. 3771–3776.
[8] L. Euler, *The Rational Mechanics of Flexible or Elastic Bodies 1638-1788: Introduction to Vol. X and XI*. Berlin, Germany: Springer, 1980.
[9] R. Levien, "The elastica: A mathematical history," *Elect. Eng. Comput. Sci. Univ. California Berkeley*, vol. 70, 2008.
[10] E. H. Dill, "Kirchhoff's theory of rods," in *Archive for Hist. of Exact Sci.*, 1992, vol. 44, no. 1, pp. 1–23. [Online]. Available: http://www.jstor.org/stable/41133926
[11] J. Till and D. C. Rucker, "Elastic rod dynamics: Validation of a real-time implicit approach," in *Proc. 2017 IEEE/RSJ Int. Conf. Intell. Robots Syst.*, 2017, pp. 3013–3019.
[12] N. Nakagawa and H. Mochiyama, "Real-time shape estimation of an elastic rod using a robot manipulator equipped with a sense of force," in *Proc. 2018 IEEE/RSJ Int. Conf. Intell. Robots Syst.*, 2018, pp. 8067–8073.
[13] T. Bretl and Z. McCarthy, "Quasi-static manipulation of a Kirchhoff elastic rod based on a geometric analysis of equilibrium configurations," *Int. J. Robot. Res.*, vol. 33, no. 1, pp. 48–68, 2014. [Online]. Available: https://doi.org/10.1177/0278364912473169

[14] D. Matthews and T. Bretl, "Experiments in quasi-static manipulation of a planar elastic rod," in *Proc. 2012 IEEE/RSJ Int. Conf. Intell. Robots Syst.*, 2012, pp. 5420–5427.
[15] M. Yu, K. Lv, H. Zhong, S. Song, and X. Li, "Global model learning for large deformation control of elastic deformable linear objects: An efficient and adaptive approach," *IEEE Trans. Robot.*, vol. 39, no. 1, pp. 417–436, Feb. 2023.
[16] O. Aghajanzadeh, M. Aranda, J. A. Corrales Ramon, C. Cariou, R. Lenain, and Y. Mezouar, "Adaptive deformation control for elastic linear objects," *Front. Robot. AI*, vol. 9, 2022, Art. no. 868459.
[17] M. Yu, H. Zhong, and X. Li, "Shape control of deformable linear objects with offline and online learning of local linear deformation models," in *Proc. 2022 Int. Conf. Robot. Automat.*, 2022, pp. 1337–1343.
[18] F. Alambeigi, Z. Wang, R. Hegeman, Y.-H. Liu, and M. Armand, "Autonomous data-driven manipulation of unknown anisotropic deformable tissues using unmodelled continuum manipulators," *IEEE Robot. Automat. Lett.*, vol. 4, no. 2, pp. 254–261, Apr. 2019.
[19] S. Bouabdallah, P. Murrieri, and R. Siegwart, "Design and control of an indoor micro quadrotor," in *Proc. IEEE Int. Conf. Robot. Automat.*, 2004, vol. 5, pp. 4393–4398.
[20] H. Liu, W. Zhao, Z. Zuo, and Y. Zhong, "Robust control for quadrotors with multiple time-varying uncertainties and delays," *IEEE Trans. Ind. Electron.*, vol. 64, no. 2, pp. 1303–1312, Feb. 2017.
[21] J. Goodman and L. Colombo, "Geometric control of two quadrotors carrying a rigid rod with elastic cables," *J. Nonlinear Sci.*, vol. 32, no. 5, 2022, p. 65.
[22] T. Chen, J. Shan, and H. H. T. Liu, "Cooperative transportation of a flexible payload using two quadrotors," *J. Guidance, Control, Dyn.*, vol. 44, no. 11, pp. 2099–2107, 2021. [Online]. Available: https://doi.org/10.2514/1.G005914
[23] G. Loianno and V. Kumar, "Cooperative transportation using small quadrotors using monocular vision and inertial sensing," *IEEE Robot. Automat. Lett.*, vol. 3, no. 2, pp. 680–687, Apr. 2018.
[24] T. Chen, J. Shan, and H. H. T. Liu, "Transportation of payload using multiple quadrotors via rigid connection," *Int. J. Aerosp. Eng.*, vol. 2022, no. 1, 2022, Art. no. 2486561. [Online]. Available: https://onlinelibrary.wiley.com/doi/abs/10.1155/2022/2486561
[25] A. Tagliabue, M. Kamel, R. Siegwart, and J. Nieto, "Robust collaborative object transportation using multiple MAVs," *Int. J. Robot. Res.*, vol. 38, no. 9, pp. 1020–1044, 2019. [Online]. Available: https://doi.org/10.1177/0278364919854131
[26] H.-N. Nguyen, S. Park, J. Park, and D. Lee, "A novel robotic platform for aerial manipulation using quadrotors as rotating thrust generators," *IEEE Trans. Robot.*, vol. 34, no. 2, pp. 353–369, Apr. 2018.
[27] R. Ritz and R. D'Andrea, "Carrying a flexible payload with multiple flying vehicles," in *Proc. 2013 IEEE/RSJ Int. Conf. Intell. Robots Syst.*, 2013, pp. 3465–3471.
[28] S. V. Romadov, A. V. Kozyr, and A. G. Efromeev, "Control design for collaborative aerial transportation of flexible payload," in *Proc. IEEE 25th Int. Conf. Young Professionals Electron Devices Mater.*, 2024, pp. 1760–1765.
[29] T. Chen, J. Shan, and H. H. Liu, "Distributed control of flexible payload transportation using multiple quadrotors," in *Proc. 2021 IEEE/ASME Int. Conf. Adv. Intell. Mechatron.*, 2021, pp. 247–252.
[30] T. Lee, M. Leok, and N. H. McClamroch, "Geometric tracking control of a quadrotor UAV on SE(3)," in *Proc. 49th IEEE Conf. Decis. Control*, 2010, pp. 5420–5425.
[31] P. A. Ioannou and J. Sun, *Robust Adaptive Control*. North Chelmsford, MA, USA: Courier Corporation, 2012.
[32] L. De Branges, "The stone-weierstrass theorem," in *Proc. Amer. Math. Soc.*, vol. 10, no. 5, pp. 822–824, 1959.
[33] P. S. Diniz et al., *Adaptive Filtering.*, vol. 4, Berlin, Germany: Springer, 1997 .
[34] S. S. Haykin, *Adaptive Filter Theory*. Noida, India: Pearson Education India, 2002.
[35] J. Xu, D. S. D'Antonio, and D. Saldaña, "H-modquad: Modular multi-rotors with 4, 5, and 6 controllable DOF," in *Proc. 2021 IEEE Int. Conf. Robot. Automat.*, 2021, pp. 190–196.
[36] J. A. Preiss, W. Honig, G. S. Sukhatme, and N. Ayanian, "Crazyswarm: A large nano-quadcopter swarm," in *Proc. 2017 IEEE Int. Conf. Robot. Automat.*, 2017, pp. 3299–3304.